Materials Advances

ROYAL SOCIETY OF CHEMISTRY

PAPER

View Article Online
View Journal

Cite this: DOI: 10.1039/d5ma00628g

Optimization of the crystalline silicon surface by chemical treatment and hydrogenated amorphous silicon: a photoluminescence study

Maria B. Candeias,*[a] Ghulam Abbas,[b] Alexandr Zamchiy,[b] Rodrigo Martins,[b] Manuel J. Mendes,[b] Hugo Águas,[b] Rui N. Pereira[a] and Joaquim P. Leitão*[a]

Interfacial defects significantly impact the performance of optoelectronic devices by influencing charge carrier recombination. This work focuses on optimizing the chemical cleaning of crystalline silicon (c-Si) substrates and the passivation of surface defects with an ultrathin layer of hydrogenated amorphous silicon (a-Si:H). The study measured low-temperature photoluminescence originating mainly from c-Si as a means of evaluating the influence of surface defect density on charge carrier recombination channels. Two different concentrations of KOH (5% and 45%) were used in the process of removing defects caused by c-Si cutting and two different conditions were used in the deposition of a-Si:H (pure SiH_4 or SiH_4 diluted in 50% H_2). The thickness of the a-Si:H layer was varied, starting from ~7 nm, depending on the deposition parameters. The two types of treatments were combined with different thicknesses. The results obtained showed that, for the passivation of optical defects on the c-Si surface, the best combination is a 5% KOH concentration with the deposition of the a-Si:H layer under SiH_4 diluted in 50% H_2. It was also verified that the thickness of this amorphous layer must be sufficiently thin so that the localization of excitons/charge carriers does not negatively influence the dynamics of charge carriers, with the best results being obtained for a value of ~8.9 ± 0.2 nm. The experimental parameters identified here allow reducing the density of defects on the c-Si surface, potentially improving the performance of c-Si solar cells.

Received 11th June 2025,
Accepted 16th November 2025

DOI: 10.1039/d5ma00628g

rsc.li/materials-advances

1 Introduction

Monocrystalline silicon (c-Si) is the most widely used semiconductor material in the manufacturing of solar cells, accounting for more than 90% of the global photovoltaic market.[1] The abundance of Si in nature, combined with the maturity of c-Si cell manufacturing processes and reduction of production costs, makes it an ideal choice for large-scale applications in the renewable energy sector.[2] Despite this success, this technology has limitations that influence the power conversion efficiency. Among the limitations, one can point out the absorption coefficient that is not very high, the indirect nature of the bandgap which is reflected in the involvement of phonons in electronic transitions, and the existence of crystalline defects or contaminating materials adsorbed on the surface. Whereas the first two factors represent the intrinsic properties of Si, the latter is susceptible to innovative technological approaches that allow the reduction of its impact on the charge carrier dynamics and (non-)radiative recombination losses. In this context, two approaches have proven effective in addressing these issues: chemical surface cleaning and passivation with hydrogenated amorphous silicon (a-Si:H).[3–6]

In the semiconductor and photovoltaic industry, before device fabrication, the cleaning of c-Si wafers to remove residues at the surface, namely organic and metallic contaminants, is a crucial step to achieve devices with improved performance.[6,7] One of the most used cleaning processes involves the use of potassium hydroxide (KOH), the Radio Corporation of America (RCA) 1,2 processes, and a treatment with highly diluted hydrofluoric acid (HF). KOH smoothens the c-Si surface through the removal of damage caused by the saw during wafer cutting, the RCA1 process removes most of the organic contaminants from the c-Si surface, and the RCA2 process eliminates most ionic and metallic contamination.[8] To remove surface oxides from c-Si, which were formed during the RCA treatments, highly diluted HF is used.[9] The role of KOH fractions remains significantly

[a] Departamento de Física and I3N, Universidade de Aveiro, Campus Universitário de Santiago, 3810-193 Aveiro, Portugal. E-mail: mariabcandeias@ua.pt, joaquim.leitao@ua.pt
[b] i3N/CENIMAT, Departamento de Ciência dos Materiais, Universidade Nova de Lisboa and CEMOP/UNINOVA, Campus de Caparica, 2829-516 Caparica, Portugal

underexplored in the literature. Only a limited number of studies provide details on the specific fractions employed, and comparative analyses of substantially different KOH fractions are virtually absent.[10–13]

Reducing surface defects in c-Si wafers can also be accomplished through alternative methods beyond cleaning processes. One of the inevitable surface defects on c-Si wafers is dangling bonds. These defects create electronic states within the energy bandgap, acting as highly efficient recombination centres.[3] The passivation of the c-Si surface with an a-Si:H layer is one of the most effective strategies for neutralizing the dangling bonds. The silane radicals present in the plasma produced in plasma-enhanced chemical vapor deposition (PECVD) fill these bonds, promoting the growth of the a-Si:H layer.[14] Additionally, the hydrogen (H) present in both the plasma and the a-Si:H layer plays a relevant role by terminating dangling bonds that persist on the c-Si surface and, thus, contributes to a further decrease in carrier surface recombination and increase of effective lifetime.[3,15,16] In addition, the growth of the a-Si:H film also relieves the strain in silicon–silicon (Si–Si) bonds at the surface, reducing additional structural defects.[3] The main benefits of such a layer are the reduction of surface recombination and the creation of a potential barrier due to the beneficial alignment between the c-Si and a-Si:H bonds, promoting charge carrier separation and facilitating electrical current extraction.[3,16–21] The studies available in the literature report thickness values of the a-Si:H layer in the range of 5–50 nm, with a greater incidence in the higher end of this range.[18,21–24] However, the identification of the optimum thickness of this passivation layer is still an open question.

This study uses radiative recombination in c-Si as a probe into three central issues in the control of (non-)radiative recombination channels in silicon-based solar cells. Firstly, it will examine how the percentage of KOH (5% and 45%) used to remove surface damage in c-Si affects the electronic energy level structure related to surface defects and, therefore, the charge carrier recombination channels. Next, the impact on these channels of the deposition of an a-Si:H layer in two different environments, pure silane (SiH_4) or SiH_4 diluted in 50% H_2 at the surface of c-Si, will be studied. Finally, the influence of the thickness of the a-Si:H layer on the recombination channels will be addressed.

2 Experimental details

2.1 Substrate cleaning treatment

Fifteen n-type c-Si samples with an ⟨100⟩ orientation, a thickness of 120 μm, and a resistivity of 1–10 Ω cm were cut from the same wafer. No significant morphological differences were observed between samples. Three of these samples, designated as S0, S1, and S2, served as reference substrates without the deposition of a-Si:H. These three substrates underwent RCA cleaning processes followed by immersion in 5% HF for 1 minute to remove the surface oxide layer. In the first step of the cleaning process (RCA1), the solution consisted of H_2O/NH_4OH 27%/H_2O_2 30% (5 : 1 : 1), whereas in the second step (RCA2), a fresh solution of H_2O/HCl 27%/H_2O_2 30% (6 : 1 : 1) was prepared and heated to 70 °C. After the last step (5% HF), the three reference substrates were subjected to different treatments with/without KOH: the S0 substrate did not undergo any KOH treatment; S1 was etched in a 45% aqueous solution of KOH; S2 was etched in a 5% aqueous solution of KOH. Both etching processes were carried out at 45 °C for 5 minutes with ultrasonication.

Table 1 Experimental conditions for the chemical treatment of the c-Si surface and for the deposition of the a-Si:H layer. The etching was performed with RCA1 and RCA2 cleaning processes; immersion in 5% HF for 1 minute; 5% or 45% aqueous solution of KOH, heated to 45 °C for 5 minutes with ultrasonication. The deposition of the a-Si:H layers was done in pure SiH_4 or SiH_4 diluted in 50% H_2. The particular KOH concentration and a-Si deposition conditions are highlighted for each sample. d_{TL} denotes the measured thickness obtained from spectroscopic ellipsometry measurements

Sample	KOH	a-Si:H deposition	d_{TL} (nm)
S3.1	5%	SiH_4	6.8 ± 0.1
S4.1			13.8 ± 0.8
S5.1			18.7 ± 0.4
S7.1		SiH_4 and 50% H_2	8.9 ± 0.2
S8.1			18.5 ± 0.3
S9.1			29.2 ± 0.6
S3.2	45%	SiH_4	7.2 ± 0.2
S4.2			12.0 ± 0.1
S5.2			15.8 ± 0.2
S7.2		SiH_4 and 50% H_2	6.9 ± 0.1
S8.2			15.6 ± 0.2
S9.2			18.6 ± 0.2

Regarding the remaining twelve samples, before the deposition of the a-Si:H layer, they were divided into two sets of samples (6 samples each), one being subjected to treatment with 5% KOH and the other to treatment with 45% KOH. The other steps (involving RCA1, RCA2 and 5% HF treatments) of the cleaning process were the same as used for the S0, S1, and S2 substrates. More details are presented in Table 1.

2.2 a-Si:H deposition

a-Si:H layers were deposited on twelve c-Si substrates by radio frequency PECVD (RF-PECVD) using an Elettrovara deposition system equipped with a load lock chamber. The deposition of the a-Si:H layers was performed using two different optimized conditions: (i) pure SiH_4 and (ii) SiH_4 diluted in 50% H_2. Before deposition, the substrates were heated for 30 minutes to reach a substrate temperature of 185 °C, while the base pressure in the chamber reached $\sim 10^{-7}$ mbar. All depositions were performed at an inter-electrode distance of 15 mm and an electrode area of 144 cm^2. The deposition power density for both films was 34.7 mW cm^{-2}, while the deposition pressures were 80 Pa and 27 Pa for pure and diluted SiH_4, respectively. Hydrogen dilution (DH) was calculated using $DH = (F_{H_2}/F_{gas}) \times 100$, where F_{H_2} represents the hydrogen flow in sccm, and F_{gas} is the total gas flow, including SiH_4 and H_2.

For each combination of substrate chemical treatment and a-Si:H deposition conditions, three samples with different

a-Si:H thicknesses, which starts at ∼7 nm, were prepared. Table 1 summarizes the experimental conditions for the preparation of the twelve samples. The percentage of KOH used for the chemical treatment (5% or 45%) and the environment (pure SiH_4 or SiH_4 diluted in 50% H_2) for the a-Si:H deposition are highlighted for each sample. Samples subjected to treatment with 5% KOH (45%) have identification ending in .1 (.2).

The thickness of the a-Si:H layers was assessed using spectroscopic ellipsometry (SE), as this optical technique is more sensitive to small variations in this physical parameter in ultrathin layers, than other electron microscopy-based techniques.[25–27] SE measurements were performed using a Jobin Yvon UVISEL DH10 ellipsometer. The experimental data were modeled with the Tauc–Lorentz (TL) model,[28] using a two-layer sample model: the substrate (c-Si) plus the a-Si:H layer. More details are presented in the SI. Table 1 presents the experimental thickness of the a-Si:H layer for each sample.

2.3 Physical characterization

PL measurements were carried out using a Bruker Vertex 80v Fourier transform infrared (FTIR) spectrometer equipped with an InGaAs detector. The samples were inserted in a nitrogen gas flow cryostat (OptistatCF, Oxford Instruments) which allows changing the sample temperature in the range of 70–300 K. The excitation source was the 457.9 nm (DPSS laser, CVI Melles Griot)) or 532 nm (MGL-F-532, CNI) laser lines, and the laser power (P) was measured at the front of the cryostat window by means of an optical power meter (842-PE, Newport), equipped with a Si detector (818-SL, Newport). The diameter of the laser spot was approximately 1 mm.

Due to the much lower a-Si:H layer thickness compared to the thickness of the c-Si substrate, the optical penetration depth (δ) of the laser light is calculated by considering only the absorption coefficient (α) of the c-Si. δ determines how deeply the laser light can probe the material and corresponds to the distance at which the light intensity decays to $1/e$ of its initial value. δ is defined as follows:[29]

$$\delta = \frac{1}{\alpha}. \quad (1)$$

According to Schinke *et al.*,[30] for λ = 457.9 nm, c-Si at 295 K has $\alpha \simeq 2.161 \times 10^4$ cm^{-1}, whereas for λ = 532 nm, $\alpha \simeq 8252$ cm^{-1}. The corresponding values of δ are 463 nm and 1.21 μm, respectively.

3 Results and discussion

Fig. 1(a) shows the PL spectra for substrates S0, S1 and S2 after the cleaning treatment of the c-Si samples. The difference between the substrates lies in the KOH treatment applied during the cleaning process: the substrate S0 did not undergo any KOH treatment, while S1 and S2 were treated with 45% and 5% KOH, respectively. The luminescence for all substrates exhibits characteristics typical of bulk c-Si. In the energy range of ∼1.03–1.14 eV, several narrow excitonic lines are observed. These lines correspond to the radiative recombination of free or bound excitons in c-Si, involving one or two phonons: transverse acoustic (TA), transverse optical (TO) and optical phonon located at the center of the Brillouin zone (O^{Γ}).[31,32] In the lower energy region, the luminescence from a point defect in c-Si, the P center, is observed.[33] It is characterized by a zero-phonon line at 0.767 eV and a vibronic band for lower energies. The P center is commonly associated with the irradiation of c-Si with high-energy ionized particles and with the presence of C and O impurities in the lattice.[33–37] Although the creation of this optical center was unintentional and is a consequence of the a-Si:H layer deposition method,[38,39] its presence in the luminescence of our samples provides an additional means of analysing the mechanisms of charge carrier recombination,

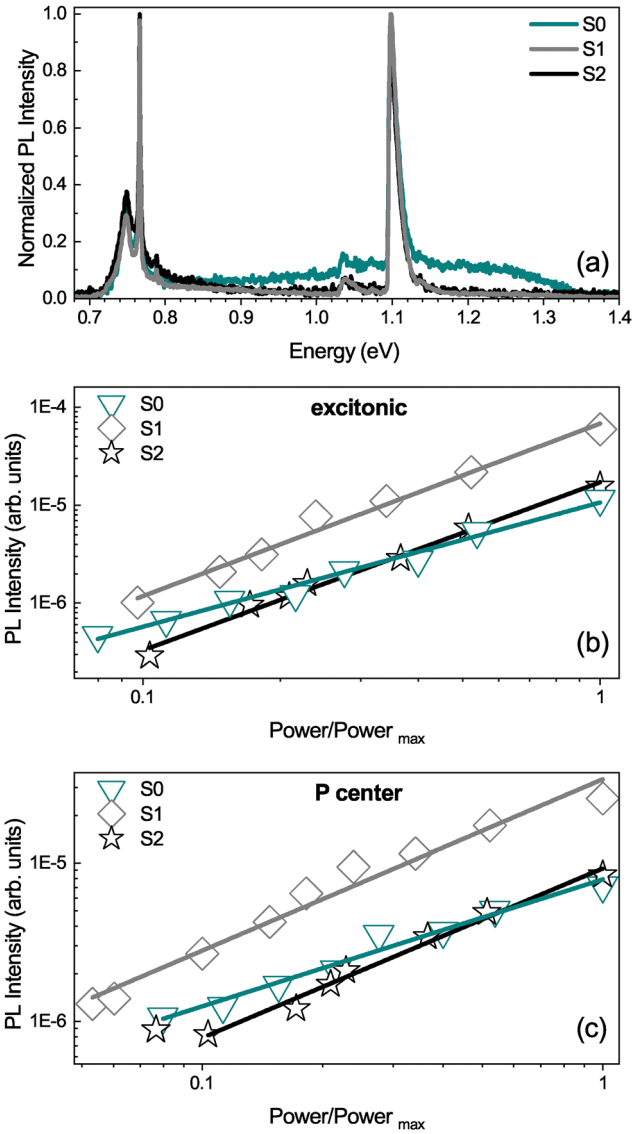

Fig. 1 (a) PL spectra for samples S0, S1 and S2. The spectra were measured at 70 K, under an excitation wavelength of 457.9 nm. (b) Excitation power dependence of the PL intensity for the excitonic luminescence for S0, S1, and S2 samples. (c) Excitation power dependence of the PL intensity for the P center for S0, S1, and S2 samples. The solid lines represent the fits of eqn (2) to the experimental data.

whether radiative or non-radiative. Therefore, the P center also contributes to discussion of the electronic properties of the c-Si/a-Si:H interface. Additionally, we must note that the shape of the PL spectra from the bare substrates suggests the presence of a broad band with a low relative intensity, underneath the excitonic luminescence and the P center. This broad band is particularly prominent in sample S0.

Defects that influence luminescence are those that create energy levels within the band gap, giving rise to radiative or non-radiative recombination channels. One possible origin for them is the damage at the Si surface resulting from saw cutting. SI presents scanning electron microscopy and atomic force microscopy images that show that there is surface damage after cutting. The images also show that after the 5% KOH treatment, small pyramids appear with base edges in the ⟨100⟩ orientation and lateral faces in the ⟨111⟩ orientation, whereas after the 45% KOH treatment, the surface appears flat after chemical treatment. These results confirm that both KOH treatments are effective in removing the saw damage. An in-depth analysis of the influence of chemical treatments on the morphology of the c-Si surface is beyond the scope of this work and will be presented elsewhere.[40]

Comparison of the luminescence between the three substrates suggests that the absence of KOH treatment is reflected in the appearance of many radiative recombination centers that contribute to the appearance of the broad band. Since the role of KOH treatment is to remove surface damage caused by the saw, the results suggest that the radiative channels contributing to the previous broad band are related to this damage. Regarding the signal-to-noise ratio (SNR), substrate S1 presents the highest value (144) whereas the other two substrates exhibit similar values: 30 for S2 and 27 for S0.

Fig. 1(b) and (c) present, for the substrates S0, S1 and S2, the dependence on the excitation power (P) of the PL integrated intensity (I) of the two types of luminescence discussed previously: (i) the excitonic luminescence corresponding to the three phonon (TA, TO, and TO + O^{Γ}) assisted free or bound exciton recombinations and (ii) the P center. The intensity was always determined by assuming as a baseline the broad band parametrized by a smooth curve and calculating the integrated intensity of the excitonic luminescence and the P center. In both cases, the intensity of the luminescence increases with the excitation power regardless of the experimental substrate preparation conditions. The experimental points were adjusted with the power law:[41–46]

$$I \propto P^{m}, \tag{2}$$

where m is an adjustable parameter representing the slope in the log(I)–log(P) plot. The estimated m values for each excitonic luminescence and P center are shown in Table 2. In the excitonic case, values of 1.27 ± 0.06, 1.8 ± 0.1 and 1.72 ± 0.07 were obtained for substrates S0, S1 and S2, respectively. In the case of the P center, the values are 0.80 ± 0.05, 1.08 ± 0.07 and 1.07 ± 0.06 for substrates S0, S1 and S2, respectively. According to the Schmidt model,[41] values of $m > 1$ are characteristic of the recombination of non-localized charge carriers, values of $m < 1$ are typical of radiative channels involving defects, and values of $m \sim 1$ are commonly ascribed to the radiative recombination of charge carriers with some degree of localization. Also, values close to 1 are in agreement with a monomolecular recombination mechanism as the dominant one.[47] The estimated m values for the excitonic luminescence are in agreement with the involvement of excitons. In the case of the P center, they are very similar to the S1 and S2 substrates and significantly higher when compared to the S0 substrate. These results indicate that, without the KOH treatment, the charge carriers are more localized, which is compatible with a higher density of defects at the c-Si surface. Therefore, the relevance of this treatment in reducing the defect density on the c-Si surface is clearly demonstrated.

Table 2 Estimated m values for S0, S1 and S2 substrates from the dependence on the excitation power of the excitonic luminescence and the P center, using an excitation wavelength of 457.9 nm

Substrate		m
S0	Excitonic	1.27 ± 0.06
	P center	0.80 ± 0.05
S1	Excitonic	1.80 ± 0.10
	P center	1.08 ± 0.07
S2	Excitonic	1.72 ± 0.07
	P center	1.07 ± 0.06

Regarding the remaining twelve samples, the combination of the percentage of KOH in the substrate cleaning treatment, a-Si:H deposition conditions, and the a-Si:H layer thickness, which allows the optimization of the passivation of the c-Si surface with a-Si:H, was investigated. The starting point for all samples was a similar level of damage due to initial wafer cutting and the same three steps in the substrate cleaning treatment: RCA1, RCA2, and 5% HF. Fig. 2(a) shows the overlap of PL spectra measured for substrate S2 and for samples with a 5% KOH step in the substrate cleaning treatment and the deposition of the a-Si:H layer in the pure SiH_4 environment (S3.1, S4.1, and S5.1). With the addition of 6.8 ± 0.1 nm of a-Si:H (S3.1), the luminescence is dominated by the recombination of free/bound excitons in c-Si and by the P center. The shape of the spectrum is compatible with the presence of a broad band in the energy range of ∼0.7–1.2 eV with a quite low relative intensity. Compared to the luminescence measured for the substrate (S2), a large increase in the SNR is observed. For thicker a-Si:H layers (S4.1, S5.1), the existence of a broad and structured band in the energy range of ∼0.7–1.4 eV is evident, characterized by an abrupt decrease in the luminescence intensity for energies above ∼1.22 eV. For a thickness of 13.8 ± 0.8 nm, the peak maximum occurs at ∼0.91 eV, but for the highest thickness, the peak appears at 1.17 eV. This behavior suggests that this broad band is a convolution of several radiative transitions. On the other hand, the shape of this broad band is clearly different from the possible broad band discussed previously for the substrates. It should be noted that the SNR of the luminescence for samples with an a-Si:H layer is much higher than the same ratio for the substrate luminescence, which shows a positive impact of the a-Si:H layer on the luminescence originating from c-Si.

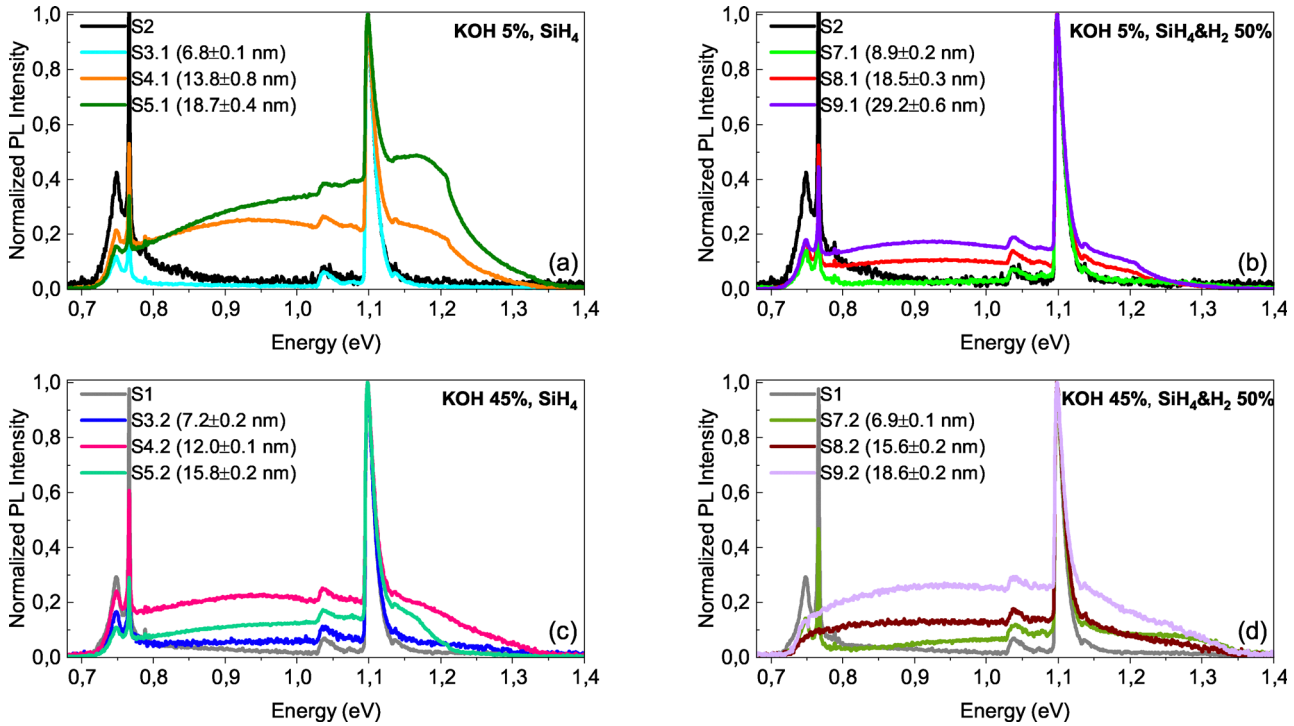

Fig. 2 PL spectra of samples without the a-Si:H layer and with different thicknesses of the a-Si:H layer, prepared under different experimental conditions: substrate cleaning treatment with 5% KOH and (a) the a-Si:H layer deposited in the pure SiH_4 environment and (b) the a-Si:H layer deposited under SiH_4 diluted in the 50% H_2 environment; substrate cleaning treatment with 45% KOH and (c) the a-Si:H layer deposited in the pure SiH_4 environment and (d) the a-Si:H layer deposited under SiH_4 diluted in 50% H_2 environment. The estimated a-Si:H layer thicknesses are shown in parentheses. The spectra were measured at ~70 K and with an excitation wavelength of 457.9 nm.

Fig. 2(b) shows a superposition of PL spectra for samples with the same substrate cleaning treatment (5% KOH) and involving the deposition of the a-Si:H layer in SiH_4 diluted in 50% H_2 environment (S7.1, S8.1, and S9.1). The observed behaviour shows that with increasing thickness of the a-Si:H layer, the relative intensity of the broad band also increases. Nonetheless, a difference is noted: with the exception of the thickness of 8.9 ± 0.2 nm, for the remainder, it can be seen that the shape of the broad band is identical to that observed in sample S4.1 with the maximum at ~0.91 eV. This broad band is attributed to the radiative recombination in the a-Si:H layer, in line with the literature.[14,15,48]

In Fig. 2(c) and (d), the PL spectra measured for samples in which the c-Si substrate underwent a cleaning treatment with 45% KOH and the deposition of the a-Si layers was done using pure SiH_4 and SiH_4 diluted in 50% H_2 environments, respectively, are presented. The overall results show a similar behaviour to the one previously described for the 5% KOH cleaning treatment of the substrate.

In the context of solar cells, it has been shown that the intensity, and consequently the SNR, of the luminescence follows the performance of the solar cell.[46,49,50] Since defects critically influence the optical and electrical properties of solar cells,[51–55] luminescence can be used as a probe for variations in defect concentration, particularly at the c-Si/a-Si:H interface. Optimizing the performance of the final device depends on the balance between the passivation of the c-Si substrate with a-Si:H and the influence of the amorphous layer on charge transport. In Fig. 2, it is observed that for samples with the two smallest thicknesses of the a-Si:H layer, the SNR ratio is clearly higher than that observed in the absence of an amorphous layer (substrates S1 and S2). In fact, the results indicate that both the SNR and the relative contributions of various radiative transitions to the luminescence are influenced by the treatment of the c-Si substrate, the deposition conditions of the a-Si:H layer, and the thickness of this layer. Furthermore, the defect density at the c-Si/a-Si:H interface is anticipated to significantly affect the dominant recombination mechanisms (radiative and non-radiative) of charge carriers in each sample.

A deeper understanding of the role of defects at the c-Si/a-Si:H interface can be inferred from the dependence on the excitation power of the integrated PL intensity, performed for the different radiative channels (excitonic luminescence and P center). The intensity integration was performed following the same procedure as that used for the substrates, *i.e.* assuming as a baseline the a-Si:H related luminescence and calculating the integrated intensity of the excitonic luminescence and the P center. Fig. 3 shows the resulting dependencies for the two smallest thicknesses of the a-Si:H layer, since it was for these two thicknesses that the highest SNR was obtained. The estimated m values are presented in Table 3. The results obtained for an excitation wavelength of 457.9 nm suggest a tendency for the value of m for the excitonic luminescence to decrease with increasing layer thickness of the a-Si:H layer. The reduction of

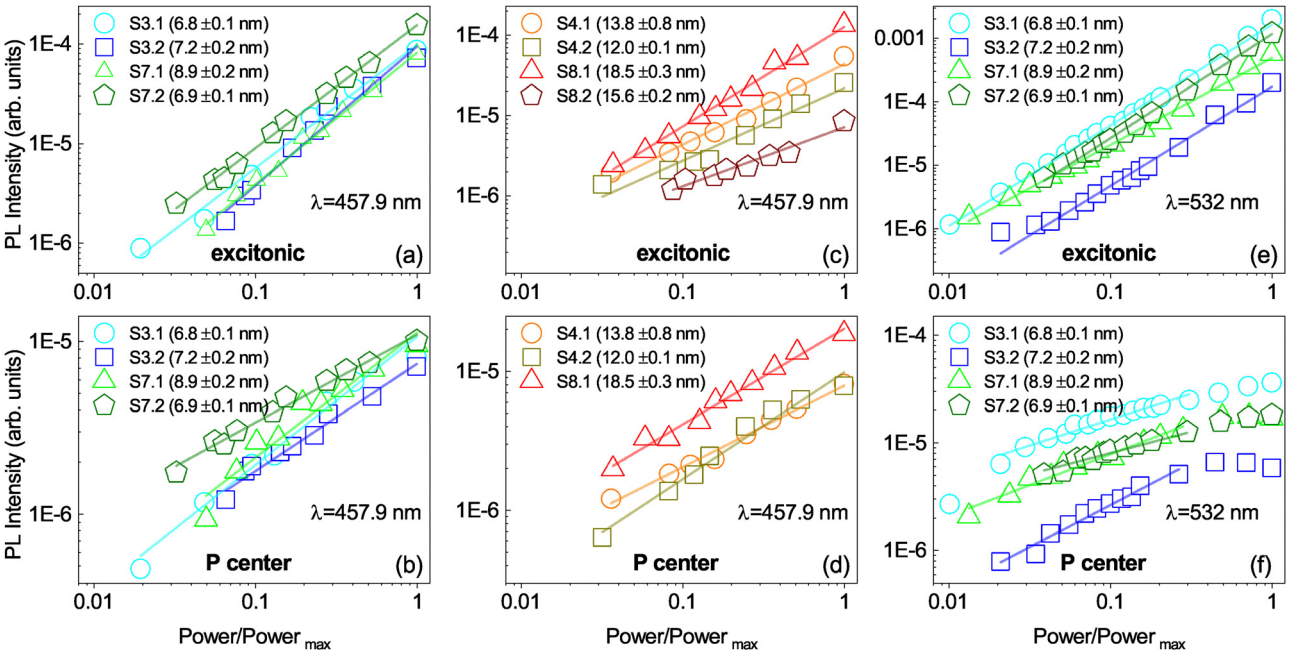

Fig. 3 Excitation power dependence of the PL intensity for the excitonic luminescence (a)–(c) and the P center (b)–(d) in c-Si. The excitation wavelengths (457.9 and 532 nm) are shown. The PL spectra measurements were carried out at 70 K. The estimated a-Si:H layer thicknesses are shown in parentheses. The solid lines represent the fits of eqn (2) to the experimental data.

Table 3 Estimated m values for samples with the two lower a-Si:H thicknesses (S3.1, S3.2, S7.1, S7.2, S4.1, S4.2, S8.1, and S8.2), measured with an excitation wavelength of 457.9 nm and estimated m values for samples with the lowest a-Si:H thicknesses (S3.1, S3.2, S7.1 and S7.2) for an excitation wavelength of 532 nm. The m values are shown for the excitonic luminescence and P center

					m	
λ (nm)	KOH	a-Si:H deposition	d_{TL} (nm)	Sample	Excitonic	P center
457.9	5%	SiH_4	6.8 ± 0.1	S3.1	1.24 ± 0.06	0.73 ± 0.05
			13.8 ± 0.8	S4.1	1.00 ± 0.05	0.59 ± 0.02
		SiH_4 and 50% H_2	8.9 ± 0.2	S7.1	1.32 ± 0.04	0.72 ± 0.07
			18.5 ± 0.3	S8.1	1.24 ± 0.04	0.69 ± 0.03
	45%	SiH_4	7.2 ± 0.2	S3.2	1.40 ± 0.09	0.61 ± 0.03
			12.0 ± 0.1	S4.2	0.90 ± 0.08	0.77 ± 0.05
		SiH_4 and 50% H_2	6.9 ± 0.1	S7.2	1.23 ± 0.02	0.51 ± 0.02
			15.6 ± 0.2	S8.2	0.74 ± 0.06	
532	5%	SiH_4	6.8 ± 0.1	S3.1	1.59 ± 0.02	0.48 ± 0.03
		SiH_4 and 50% H_2	8.9 ± 0.2	S7.1	1.37 ± 0.02	0.57 ± 0.03
	45%	SiH_4	7.2 ± 0.2	S3.2	1.56 ± 0.04	0.78 ± 0.04
		SiH_4 and 50% H_2	6.9 ± 0.1	S7.2	1.64 ± 0.03	0.45 ± 0.03

m is ascribed to greater exciton localization, which is expected to be caused by local changes in the atomic periodicity. Two effects can contribute in opposite ways to this localization. On the one hand, the passivation with the a-Si:H layer leads to the reduction of the defect density at the interface and, on the other hand, the presence of an amorphous layer modifies the atomic periodicity due to its degree of intrinsic disorder. With increasing layer thickness, it is expected that the second effect will overlap the first, resulting in increased exciton localization and a negative influence on charge carrier recombination in c-Si. Therefore, the thickness of the a-Si layer must be small enough. Interestingly, the fact that for both samples S7.1 and S8.1 the m values for the excitonic luminescence fall within the same range suggests that, for the used particular combination of the substrate cleaning treatment and a-Si:H deposition environment, the amorphous layer thickness does not significantly impact the localization of the excitons. In the case of the P center, the values of m for all investigated samples remain approximately constant, suggesting that the nature of recombination is not significantly affected by the a-Si:H layer thickness.

Considering now the samples with the smallest thickness of the a-Si:H layer, we investigated the effect of increasing the penetration depth of the excitation (λ = 532 nm), thus photogenerating charge carriers further away from the c-Si/a-Si:H interface. Fig. 3(e) and (f) show the corresponding dependencies on the excitation power of the integrated PL intensity for

the two types of radiative channels (excitonic luminescence and P center), and the estimated m values are presented in Table 3. In comparison with the previous estimated m values (for λ = 457.9 nm), an increase of m for the excitonic luminescence was observed, whereas for the P center, there was a decrease for all samples with the exception of S3.2 for which m remained approximately constant. The deviation of the power law evidenced by the experimental points for the higher excitation power values (see Fig. 3(f)), is attributed to a saturation effect due to the complete excitation of the optical centers.

The comparison of the estimated m values for the small thickness of the a-Si:H layer for the two excitation wavelengths can be interpreted in terms of the density of defects at the c-Si/a-Si:H interface. If we assume a sufficiently high density, the photoexcitation of charge carriers near the interface (λ = 457.9 nm) results in a stronger influence of defects on their (radiative or non-radiative) recombination. It is expected the occurrence of many deep-level defects within the bandgap related to these interface defects should be mostly non-radiative. The more defects present at the surface, the higher the probability of capture of charge carriers by those deep defects. On the other hand, when switching to a deeper excitation (λ = 532 nm), the influence of surface defects becomes smaller, effectively reducing the influence of defects in the region where the photogeneration occurs. Interestingly, for sample S7.1, no significant variation in the estimated m value for the excitonic luminescence was observed with increasing penetration depth of the laser excitation. This result suggests that the defect concentration at the surface must be significantly lower compared to the other three samples, which may imply that the optimal surface conditions for the c-Si/a-Si:H interface occur when c-Si is treated with 5% KOH and the a-Si:H layer is deposited in SiH_4 diluted in 50% H_2 environment.

Finally, the comparison of the estimated m values for the substrates (S1 and S2) and samples with the thinnest a-Si:H layer presented in Tables 2 and 3, respectively, reveals a decrease in the m values following the addition of the amorphous layer. As discussed above, this behaviour can be due to the presence of a non-crystalline lattice at the surface of the c-Si substrate. However, Fig. 2 clearly shows an increase of the SNR with the addition of the a-Si:H layer, evidencing effective passivation of surface defects, namely dangling bonds. Thus, the benefit of the passivation of the c-Si surface with a-Si:H is clearly demonstrated.

4 Conclusions

Interfacial defects are generally among the main causes for the underperformance of optoelectronic devices. This work provides an in-depth look at surface defect mitigation in c-Si samples, and their optical assessment *via* photoluminescence probing. The control of defects on the c-Si surface was studied by combining two approaches for removing defects on the c-Si surface. Firstly, it has shown the relevance of the KOH treatment to removal of defects created by the saw and the influence of varying the KOH concentration. Two different concentrations were used: 5% and 45%. Secondly, the deposition of an a-Si:H layer for the passivation of surface defects on c-Si was investigated using two different environments, pure SiH_4 and SiH_4 diluted in 50% H_2. The two treatments were combined to obtain four different ways of preparing a-Si:H-passivated c-Si samples. Photoluminescence of free/bound excitons and a point defect (center P) in c-Si was used to probe the influence of surface defects on the dominant recombination mechanisms. The combination of the two approaches revealed that a higher reduction in defect density is obtained for a KOH concentration of 5% in the substrate cleaning and for the deposition of the a-Si:H layer in SiH_4 diluted in the 50% H_2 environment, with a thickness of 8.9 $\pm$ 0.2 nm. The increase in the thickness of the a-Si:H layer leads to an increase in the luminescence related to this layer and to a greater localization of excitons, which proves to be detrimental to the charge transport in a solar cell. Therefore, the optimization of the passivation effect of the c-Si surface is achieved with a sufficiently small thickness of the a-Si:H layer.

Conflicts of interest

There are no conflicts to declare.

Data availability

Data for this article are either included in the manuscript or supplementary information (SI). Supplementary information: (i) details of the implementation of the Tauc–Lorentz model using a two-layer sample model, in the modeling of experimental ellipsometry data; (ii) surface morphology of the c-Si substrates evaluated by scanning electron microscopy and atomic force microscopy. See DOI: https://doi.org/10.1039/d5ma00628g.

Any additional information is available from the corresponding authors upon request.

Acknowledgements

This work received funding from FCT (Fundação para a Ciência e Tecnologia, I.P.) under the projects UID/50025 (10.54499/UID/50025/2025) and the Associate Laboratory I3N – LA/ P/0037/2020 (10.54499/LA/P/0037/2020) and by the projects FlexSolar (PTDC/CTM-REF/1008/2020) and SpaceFlex (2022.01610.PTDC, DOI: https://doi.org/10.54499/2022.01610.PTDC). J. P. Leitão acknowledges the financial support from the Project ''Agenda ILLIANCE'' [C644919832-00000035|Project no. 46], financed by PRR – Plano de Recuperação e Resiliência under the Next Generation EU from the European Union.

Notes and references

1 S. Philipps and W. Warmuth, *Photovoltaics Report*, Fraunhofer institute for solar energy systems,ise technical report, 2024.

2 M. Mikolášek, *Silicon Heterojunction Solar Cells: the Key Role of Heterointerfaces and Their Impact on the Performance*, InTech, USA, 2017.
3 M. Z. Burrows, U. K. Das, R. L. Opila, S. De Wolf and R. W. Birkmire, *J. Vac. Sci. Technol., A*, 2008, **26**, 683.
4 S. Xiao and S. Xu, *Crit. Rev. Solid State Mater. Sci.*, 2014, **39**, 277–317.
5 T. G. Allen, J. Bullock, X. Yang, A. Javey and S. De Wolf, *Nat. Energy*, 2019, **4**, 914.
6 G. Limodio, G. D'Herouville, L. Mazzarella, Y. Zhao, G. Yang, O. Isabella and M. Zeman, *Mater. Sci. Semicond. Process.*, 2019, **97**, 67.
7 H. Angermann, *Appl. Surf. Sci.*, 2008, **254**, 8067.
8 L. Zhang, W. Liu, R. Chen, J. Liu, F. Meng, Z. Liu, K. Toshima, A. Ota and T. Yoshihara, 2016 IEEE 43rd Photovoltaic Specialists Conference (PVSC), 2016, p. 0743.
9 W. Kern, *J. Electrochem. Soc.*, 1990, **137**, 1887.
10 L. A. Dobrzański, A. Drygała, K. Gołombek, P. Panek, E. Bielańska and P. Zięba, *J. Mater. Process. Technol.*, 2008, **201**, 291.
11 D. Muñoz, P. Carreras, J. Escarré, D. Ibarz, S. M. De Nicolás, C. Voz, J. M. Asensi and J. Bertomeu, *Thin Solid Films*, 2009, **517**, 3578.
12 B. Radfar, F. Es and R. Turan, *Renewable Energy*, 2020, **145**, 2707.
13 A. Sinha and M. C. Gupta, *Semicond. Sci. Technol.*, 2021, **36**, 085002.
14 R. A. Street, *Silicon Heterojunction Solar Cells: the Key Role of Heterointerfaces and Their Impact on the Performance*, Cambridge University Press, 1991.
15 R. A. Street, *Adv. Phys.*, 1981, **30**, 593.
16 H. Meddeb, T. Bearda, Y. Abdelraheem, H. Ezzaouia, I. Gordon, J. Szlufcik and J. Poortmans, *J. Phys. D: Appl. Phys.*, 2015, **48**, 415301.
17 S. De Wolf and M. Kondo, *J. Appl. Phys.*, 2009, **105**, 103707.
18 A. Illiberi, P. Kudlacek, A. H. M. Smets, M. Creatore and M. C. M. Van De Sanden, *Appl. Phys. Lett.*, 2011, **98**, 242115.
19 I. Santos, M. Cazzaniga, G. Onida and L. Colombo, *J. Phys.: Condens. Matter*, 2014, **26**, 095001.
20 M. Liebhaber, M. Mews, T. F. Schulze, L. Korte, B. Rech and K. Lips, *Appl. Phys. Lett.*, 2015, **106**, 031601.
21 L. Zhao, W. Zhang, J. Chen, H. Diao, Q. Wang and W. Wang, *Front. Energy*, 2017, **11**, 85.
22 S. Olibet, E. Vallat-Sauvain and C. Ballif, *Phys. Rev. B:Condens. Matter Mater. Phys.*, 2007, **76**, 035326.
23 S. De Wolf, B. Demaurex, A. Descoeudres and C. Ballif, *Phys. Rev. B:Condens. Matter Mater. Phys.*, 2011, **83**, 233301.
24 D. Deligiannis, J. van Vliet, R. Vasudevan, R. A. C. M. M. Van Swaaij and M. Zeman, *J. Appl. Phys.*, 2017, **121**, 085306.
25 I. An, H. V. Nguyen, N. V. Nguyen and R. W. Collins, *Phys. Rev. Lett.*, 1990, **65**, 2274–2277.
26 S. Hazra, M. Yamanaka, I. Sakata, T. Tsutsumi, T. Maeda and E. Suzuki, *Jpn. J. Appl. Phys.*, 2000, **39**, 6196.
27 A. Fontcuberta i Morral, P. Roca i Cabarrocas and C. Clerc, *Phys. Rev. B:Condens. Matter Mater. Phys.*, 2004, **69**, 125307.
28 H. Águas, V. Silva, E. Fortunato, S. Lebib, P. Roca i Cabarrocas, I. Ferreira, L. Guimarães and R. Martins, *Jpn. J. Appl. Phys.*, 2003, **42**, 4935.
29 J. Humlícek, Optical functions of the relaxed SiGe alloy, in *Properties of Silicon Germanium and SiGe: Carbon*, ed. E. Kasper and K. Lyutovich, INSPEC, The Institution of Electrical Engineers, 2000, vol. 24.
30 C. Schinke, P. Christian Peest, J. Schmidt, R. Brendel, K. Bothe, M. R. Vogt, I. Kröger, S. Winter, A. Schirmacher and S. Lim, *et al.*, *AIP Adv.*, 2015, **5**, 067168.
31 M. A. Vouk and E. C. Lightowlers, *J. Phys. C-Solid State Phys.*, 1977, **10**, 3689.
32 N. M. Santos, B. P. Falcão, J. P. Leitão, N. A. Sobolev, M. C. Carmo, N. S. Stepina, A. Yakimov and A. I. Nikiforov, *IOP Conf. Ser.:Mater. Sci. Eng.*, 2009, **6**, 012018.
33 G. Davies, *Phys. Rep.*, 1989, **176**, 83.
34 N. S. Minaev and A. V. Mudryi, *Phys. Status Solidi A*, 1981, **68**, 561.
35 G. Davies, E. C. Lightowlers, R. Woolley, R. C. Newman and A. S. Oates, *J. Phys. C-Solid State Phys.*, 1984, **17**, L499.
36 J. Wagner, A. Dörnen and R. Sauer, *Phys. Rev. B:Condens. Matter Mater. Phys.*, 1985, **31**, 5561.
37 J. Leitão, N. Santos, N. Sobolev, M. Correia, N. Stepina, M. Carmo, S. Magalhães, E. Alves, A. Novikov, M. Shaleev, D. Lobanov and Z. Krasilnik, *Mater. Sci. Eng., B*, 2008, **147**, 191–194.
38 B. Leszczynska, C. Strobel, S. Leszczynski, M. Albert, F. Stahr, J. Kuske and J. W. Bartha, Proceedings of the 35th European Photovoltaic Solar Energy Conference and Exhibition, 2018, pp. 665–667.
39 J. Wang, X. Ru, T. Ruan, Y. Hu, Y. Zhang and H. Yan, *J. Mater. Sci.: Mater. Electron.*, 2021, **32**, 25327.
40 G. Abbas, A. Zamchiy, P. Ferreira, T. Calmeiro, U. D. Menda, J. Deuermeier, T. Mateus, M. B. Candeias, R. N. Pereira, J. P. Leitão, E. Fortunato, R. Martins, M. J. Mendes and H. Águas, submitted.
41 T. Schmidt, K. Lischka and W. Zulehner, *Phys. Rev. B:Condens. Matter Mater. Phys.*, 1992, **45**, 8989.
42 J. P. Teixeira, R. A. Sousa, M. G. Sousa, A. F. da Cunha, P. A. Fernandes, P. M. P. Salomé, J. C. González and J. P. Leitão, *Appl. Phys. Lett.*, 2014, **105**, 163901.
43 N. Ben Sedrine, R. Ribeiro-Andrade, A. Gustafsson, M. R. Soares, J. Bourgard, J. P. Teixeira, P. M. P. Salomé, M. R. Correia, M. V. B. Moreira, A. G. De Oliveira, J. C. González and J. P. Leitão, *Nanoscale*, 2018, **10**, 3697.
44 J. P. Teixeira, R. B. L. Vieira, B. P. Falcão, M. Edoff, P. M. P. Salomé and J. P. Leitão, *J. Phys. Chem. C*, 2020, **124**, 12295.
45 B. P. Falcão, J. P. Leitão, L. Ricardo, H. Águas, R. Martins and R. N. Pereira, *Appl. Mater. Today*, 2021, **23**, 101071.
46 M. B. Candeias, T. V. Fernandes, B. P. Falcão, A. F. Cunha, J. M. V. Cunha, J. Barbosa, J. P. Teixeira, P. A. Fernandes, M. Peres, K. Lorenz, P. M. P. Salomé and J. P. Leitão, *J. Mater. Sci.*, 2023, **58**, 16385.
47 B. P. Falcão, J. P. Leitão, L. Ricardo, H. Águas, R. Martins and R. N. Pereira, *Appl. Mater. Today*, 2021, **23**, 101071.
48 D. Engemann and R. Fischer, *Phys. Status Solidi B*, 1977, **79**, 195–202.

49 T. V. Fernandes, P. T. Patrício, A. F. da Cunha, J. Gaspar, N. Catarino, M. Peres, K. Lorenz, J. P. Teixeira, P. M. P. Salomé and J. P. Leitão, *ACS Appl. Energy Mater.*, 2025, **8**, 2767–2778.
50 T. V. Fernandes, J. Gomes, J. Gaspar, P. T. Patrício, B. P. Falcão, A. F. da Cunha, N. Catarino, J. G. Marques, M. Peres, K. Lorenz, J. P. Teixeira, P. M. P. Salomé and J. P. Leitão, *J. Phys.: Energy*, 2025, **7**, 035021.
51 J. P. Teixeira, P. M. P. Salomé, B. Alves, M. Edoff and J. P. Leitão, *Phys. Rev. Appl.*, 2019, **11**, 054013.
52 D. Abou-Ras, N. Schäfer, C. J. Hages, S. Levcenko, J. Márquez and T. Unold, *Sol. RRL*, 2018, **2**, 1700199.
53 Y. J. Song, M. R. Park, E. Guliants and W. A. Anderson, *Sol. Energy Mater. Sol. Cells*, 2000, **64**, 225.
54 A. Amaral, G. Lavareda, C. N. De Carvalho, P. Brogueira, P. M. Gordo, V. S. Subrahmanyam, C. L. Gil, M. D. Naia and A. P. de Lima, *Thin Solid Films*, 2002, **403**, 539.
55 Y. Liu, Y. Li, Y. Wu, G. Yang, L. Mazzarella, P. Procel-Moya, A. C. Tamboli, K. Weber, M. Boccard and O. Isabella, *Mater. Sci. Eng., R*, 2020, **142**, 100579.